LANGMUIR

Subscriber access provided by BNL Research Library

Interfaces: Adsorption, Reactions, Films, Forces, Measurement Techniques, Charge Transfer, Electrochemistry, Electrocatalysis, Energy Production and Storage

Mechanistic study of lead adsorption on activated carbon

Qiantao Shi, George E. Sterbinsky, Valentina Prigiobbe, and Xiaoguang Meng

Langmuir, **Just Accepted Manuscript** • DOI: 10.1021/acs.langmuir.8b03096 • Publication Date (Web): 16 Oct 2018

Downloaded from http://pubs.acs.org on October 18, 2018

Just Accepted

"Just Accepted" manuscripts have been peer-reviewed and accepted for publication. They are posted online prior to technical editing, formatting for publication and author proofing. The American Chemical Society provides "Just Accepted" as a service to the research community to expedite the dissemination of scientific material as soon as possible after acceptance. "Just Accepted" manuscripts appear in full in PDF format accompanied by an HTML abstract. "Just Accepted" manuscripts have been fully peer reviewed, but should not be considered the official version of record. They are citable by the Digital Object Identifier (DOI®). "Just Accepted" is an optional service offered to authors. Therefore, the "Just Accepted" Web site may not include all articles that will be published in the journal. After a manuscript is technically edited and formatted, it will be removed from the "Just Accepted" Web site and published as an ASAP article. Note that technical editing may introduce minor changes to the manuscript text and/or graphics which could affect content, and all legal disclaimers and ethical guidelines that apply to the journal pertain. ACS cannot be held responsible for errors or consequences arising from the use of information contained in these "Just Accepted" manuscripts.

ACS Publications

is published by the American Chemical Society. 1155 Sixteenth Street N.W., Washington, DC 20036

Published by American Chemical Society. Copyright © American Chemical Society. However, no copyright claim is made to original U.S. Government works, or works produced by employees of any Commonwealth realm Crown government in the course of their duties.

Mechanistic study of lead adsorption on activated carbon

Qiantao Shi[a], George E. Sterbinsky[b], Valentina Prigiobbe[a], and Xiaoguang Meng[a]*

[a]Center for Environmental Systems, Stevens Institute of Technology, Hoboken, New Jersey 07030, United States
[b]Advanced Photon Source, Argonne National Laboratory, Argonne, Illinois 60439, USA

Tel: 001 201-216-8014; Fax: 001 201-216-8303

E-mail: xmeng@stevens.edu

Abstract

Activated carbon (AC) is a carbonaceous material broadly applied in filters to remove lead (Pb(II)) from drinking water through adsorption. However, the chemical interactions between Pb(II) and the reactive sites on AC or other carbonaceous materials are not well understood, yet. The understanding of the mechanism of Pb(II) adsorption onto AC would allow to optimally design AC-based materials even in the presence of a complex liquid phase. Here, the interaction between Pb(II) and functional groups on AC was investigated at the molecular scale to help identifying the chemical reactions at the solid-liquid interface. Spectroscopic analyses and chemical quantum calculations were performed and indicated the formation of monodentate mononuclear Pb(II)-phenol and bidentate mononuclear Pb(II)-carboxyl complexes on AC. Competitive adsorption behavior was observed between Pb(II) and calcium (Ca(II)), because of their similar adsorption configurations on AC. In contrast, anions, including sulfate and phosphate, were observed to enhance Pb(II) adsorption on AC by forming ternary complexes. Based on these observations, a new surface complexation model of Pb(II) adsorption onto AC was formulated and validated with batch tests. Overall, this work presents a new set of chemical reactions at the solid-liquid interface between Pb(II) and AC under various conditions of interest for the application of AC or other carbonaceous materials in water treatment.

Keywords: Activated carbon; lead; density functional theory; inner-sphere complex; spectroscopy.

Introduction

Drinking water becomes contaminated with divalent lead (Pb(II)) as it travels through lead or galvanized service lines (LSLs or GSLs) on individual properties and lead plumbing fixtures inside homes. Lead can be found in drinking water either dissolved or as particulate[1, 2]. Generally, corrosion inhibitors (e.g., phosphate or poly-phosphate) are used to inhibit the dissolution of pipe walls, reducing also the risk of the presence of soluble Pb(II) within the water. However, even in the presence of corrosion inhibitors, soluble Pb(II) can exceed the quality standards of drinking water[2]. At concentrations as low as 10 μg/L[3, 4], Pb(II) can pose a significant health threat, in particular to pregnant women and young children. Currently, activated carbon (AC) is the conventional material used for the removal of soluble Pb(II) from drinking water. The studies regarding the adsorption of Pb(II) on AC has been widely reported[5-9]. By analyzing the change of pH during adsorption process, and the characterizations using X-ray photoelectron spectroscopy (XPS) and Fourier transformed infrared spectroscopy (FTIR), Pb(II) was observed to form inner-sphere complexes with the functional groups on AC.[9, 10] However, the mechanism of interaction of Pb(II) and AC, in particular, the adsorption structure is not well understood yet. Meanwhile, although previous studies indicated the competitive effect of calcium (Ca(II)) and the enhanced effect of anions on Pb(II) adsorption by activated carbon[11, 12], the mechanism underlying this experimental phenomenon is also not well studied. The understanding of the adsorption mechanism would allow to optimally design AC-based

materials, in particular in the presence of a complex aqueous solutions. To identity the mechanism, chemical reactions at the solid-liquid interface Pb(II) and AC must be formulated. This can be achieved through the study at the molecular level of the adsorption process both theoretically and experimentally.

Quantum chemical calculations using density functional theory (DFT) have been performed to investigate the geometric structure of Pb(II) adsorption onto various adsorbents[13-18] under several thermodynamic conditions, providing insight into the interaction between Pb(II) and adsorbents under conditions which are not easily to be tested in the laboratory. DFT is a valuable tool to study the mechanisms of interaction at the solid-liquid interface. In the work by Mason *et al.*[17], it was found that the adsorption of Pb(II) onto goethite is more favorable than onto alumina due to the favorable bonding interaction of Pb(II) with the d bands of Fe. More recently, reported DFT calculation studies of Pb(II) adsorption on carbonaceous materials proved that oxygen- containing functional groups were the active adsorption sites for Pb(II)[13-16].

The atomic-level structures of Pb(II) adsorption on metal oxides have been studied by EXAFS in a number of previous works[19-22]. Meanwhile, in-situ flow cell ATR-FTIR spectroscopy is usually combined with EXAFS to explore the simultaneous adsorption of anions and cations[21, 23-26]. Through the combination of those two techniques, formation of a ternary surface complex of Pb(II) and SO_4^{2-} on goethite was observed in previous studies [21, 27]. To the best of our knowledge, the adsorption of Pb(II) onto AC has been never

investigated using a combination of EXAFS and in-situ ATR-FTIR techniques and accounting for the presence of co-existing anions such as SO_4^{2-} and $H_2PO_4^-$.

In this paper, a study combining DFT calculations with spectroscopic methods, including pellet-FTIR, EXAFS and *in situ* ATR-FTIR techniques, is presented. The results allow to gain an insight into the fundamental physicochemical mechanism underlying the adsorption of Pb(II) onto AC under various conditions. The structures of Pb(II) adsorption identified at the molecular scale were then used to develop a surface complexation model (i.e. charge distribution multisite ion complexation, CD-MUSIC), which was validated with batch tests.

Materials and methods

DFT calculations

Periodic *ab initio* DFT calculations were performed using the Vienna ab initio Simulation Package (VASP)[28]. Simulations were run using the Perdew−Burke−Enzerhoff (PBE)[29] generalized gradient approximation (GGA) with the motion effects of the core electrons and their nuclei replaced by an effective core potential or pseudopotential. The pseudopotential employed in this work was based on the projector-augmented wave (PAW) type[30, 31] with an optimized cutoff energy of 450 eV. The *k*-point mesh of 4×4×1 for the Brillouin zone (BZ) was chosen according to a Monkhorst−Pack[32] grid. The effect of the solvation was considered by an implicit solvent model using VASPsol[33, 34]. The long-range dispersion correction was also considered by adding the Becke−Johnson (BJ) damped

atom-pair wise potential (D3BJ)[35, 36]. The convergence criteria for electronic and ionic minimization is set to 10^{-4} eV and 0.01 eV/Å, respectively. The method of Gaussian smearing a width of 0.05 eV was used to broaden the energy near Fermi level for calculating the partial occupancies. The AC model was built on the basis of its reported amorphous structure, which consists of 42 carbon atoms, including five-, six-, and seven-member carbon rings[37, 38] (shown in Figure S1). The geometric optimized AC bulk unit cell has no symmetry at all, showing a P1 space group. The AC surfaces with phenol (COH) and carboxyl (COOH and COO^-) groups were then modeled using three-dimensional periodic slabs with additional carboxyl and phenol groups on AC surface, and with 12 Å of vacuum space between them. The cell size was also optimized, showing lengths of 7.798, 7.416, and 16.852 Å in A, B, and C directions, respectively. During the DFT calculation, Pb(II) was surrounded by two hydroxyl groups and six water molecules ($Pb(OH)_2(OH_2)_6$, Table S1). These two surrounding hydroxyl groups neutralized the total charge of the unit cells, which is similar to previous study for Pb(II) adsorption on metal oxides[17, 18]. In the DFT calculation for the deprotonated carboxyl groups, the proton was put upon the surface with a distance larger than 5 Å. In the DFT calculation for Pb(II) complexation with phenol and carboxyl groups on AC surface, the hydroxyl ions and water molecules were also put upon the surface with a distance larger than 5 Å. Therefore, the unit cell charge was always neutralized during the DFT calculation.

Chemicals

Stock solutions of 1 g/L Pb(II) and Ca(II) were prepared by dissolving lead nitrate

($Pb(NO_3)_2$) and calcium chloride ($CaCl_2$) in 1 % nitric acid (HNO_3) solution, respectively. Stock solutions of 1 g/L sulfate (SO_4^{2-}) and phosphate ($H_2PO_4^-$) (as P) were prepared by dissolving disodium sulfate (Na_2SO_4) and disodium hydrogen phosphate (Na_2HPO_4) into DI water (i.e., conductivity higher than 18.2 MΩ·cm), respectively. All chemicals used were reagent grade and purchased from Fisher or Sigma-Aldrich (U.S.A.). Activated carbon was obtained from Nichem Company (U.S.A.). The AC was sieved, and the fraction between 30 and 50 mesh (i.e. with openings of 0.3 and 0.6 mm, respectively) was used in this study, showing a bulk density of 0.49 g/mL. The specific surface area was measured by applying Brunauer–Emmett–Teller (BET) equation for the N_2 adsorption data using an ASAP 2010 (Micrometrics, U.S.A.) and resulted to be 997 m^2/g. The average pore size of 4.7 nm was determined by the BJH (Barrett, Joyner, and Halenda) method.

Sample preparation for spectroscopic analyses

Table 1 lists the aqueous solutions used in the spectroscopic tests. For the sake of simplicity, in the rest of the paper, the solutions will be referred to by the symbols introduced in this table. The pH of 5 was selected to avoid the possible formation of precipitate.

Pellet-FTIR analysis

Samples for pellet-FTIR analysis were prepared by mixing 0.1 g of AC in 1 L of Sol 1, Sol 2, or Sol 3, as listed in Table 1. The pH of the solutions was also maintained at 5.0 ± 0.2. After four hours of mixing, the solids were separated from the solution by filtration

using a 0.2 μm glass fiber, rinsed with 100 mL DI water, and freeze-dried under vacuum. The dry solids were ground, sieved (< 200 mesh), mixed with potassium bromide (KBr), and then pressed into a pellet. Pellet-FTIR spectra of the dry samples were collected using a spectrometer (Thermo-Nicolet Nexus IS50, U.S.A.) equipped with a liquid-nitrogen-cooled mercury-cadmium-telluride (MCT) detector. The spectra were collected in transmission mode at a resolution of 4 cm^{-1}, and 512 scans were recorded in the 4000-650 cm^{-1} range.

Table 1. Solutions used for the spectroscopic tests.

Solution	Composition	Analytical techniques
Sol 1	0.01 M NaCl	Pellet-FTIR
Sol 2	1 mg/L Pb(II), 0.01 M NaCl	Pellet-FTIR, EXAFS
Sol 3	50 mg/L Ca(II), 0.01 M NaCl	Pellet-FTIR, EXAFS
Sol 4	30 mg/L SO_4^{2-}, 0.01 M NaCl	*In situ* ATR-FTIR
Sol 5	30 mg/L SO_4^{2-}, 1 mg/L Pb(II), 0.01 M NaCl	EXAFS, *in situ* ATR-FTIR
Sol 6	1 mg/L $H_2PO_4^-$ (as P), 0.01 M NaCl	*In situ* ATR-FTIR
Sol 7	1 mg/L $H_2PO_4^-$ (as P), 1 mg/L Pb(II), 0.01 M NaCl	EXAFS, *in situ* ATR-FTIR

XAS analysis

Samples for XAS analysis were prepared by mixing Sol 2, Sol 3, Sol 5, and Sol 7 (as reported in Table 1) with 0.1 g/L of AC for 4 hours. The NaOH and HCl solutions were used to maintain the pH of the Sol 2, 3, 5, and 7 at 5.0 ± 0.2. The solid for the measurements was separated by filtration and freeze-dried under vacuum. The Pb L_{III}-edge (13,055 eV) and Ca K-edge (4,038.5 eV) spectra were collected at beamline 9-BM at the Advanced Photon Source (APS, Argonne National Laboratory, U.S.A.). An energy range of -200−1000 eV, relative to the Pb L_{III} and Ca K-edges, was used to acquire the spectra with a standard Lytle detector at room temperature. Three to eight scans were collected from

each sample, inspected for overall quality, and averaged to improve the signal/noise ratio. The EXAFS data analysis was performed using the ATHENA and ARTEMIS programs in the Demeter computer package[39, 40]. The procedure followed during the analysis of the data was similar to that used in our previous works[41, 42], and details are provided in the supporting information (SI) document.

***In situ* flow cell ATR-FTIR analysis**

The *in situ* flow cell ATR-FTIR measurements were performed using the spectrometer and MCT detector, mentioned above, with an additional horizontal attenuated total reflectance (HATR) cell (PIKE Tech). A multibounce ZnSe ATR crystal with 45° beveled faces (infrared angle of incidence, θ) was used, and the infrared spectra were collected using 512 scans per spectrum at a resolution of 4 cm^{-1}. The sample preparation and collection of the spectra of SO_4^{2-} and $H_2PO_4^-$ adsorption onto AC with/without Pb(II) were similar to those described in our previous work[41]. Briefly, an adsorbent film was deposited on the ZnSe crystal by applying 500 µL of 2.5 g/L of AC followed by drying at room temperature. Prior to use, the film was rinsed with DI water to remove loosely deposited particles. A solution containing 0.01 mol/L of NaCl was supplied to the flow cell at a rate of 0.5 mL/min until there was no further change in the IR spectra. A background spectrum of the absorbance of the ZnSe crystal and the deposited AC with flowing NaCl solution was collected. Then, solutions of Sol 4 through Sol 7 (as reported in Table 1) were adjusted at pH 5 and flowed through the cell. Spectra were recorded as a function of time until the adsorption reached equilibrium (~ 5 h). All samples were purged with N_2 in the dark, during the data collection. Second-order derivatives were used to locate the peak positions.

Batch experiment

Tests of Pb(II) adsorption on AC at different pH were carried out with and without Ca(II), SO_4^{2-}, and $H_2PO_4^-$ to study the effect of these ions on Pb(II) adsorption. Specifically, a concentration of 1 mg/L of Pb(II) in a 50 mL 0.01 M NaCl solution was prepared with either 50 mg/L Ca(II), 30 mg/L SO_4^{2-}, or 1 mg/L $H_2PO_4^-$ (P) at pH 3. Then, the prepared solution was placed in capped 50 mL centrifuge tubes with an amount of 5 mg of AC. The suspension pH was adjusted to 3, 4, 5, 6, 7, and 8, and then mixed using a rotator at 30 rpm until equilibrium. Preliminary kinetic tests showed that after 4 hours the reaction could reach equilibrium, agreed well with previous kinetic studies of Pb(II) adsorption on AC.[43-46] At the end of this time period, the pH was measured. Samples were collected by filtering using 0.2 μm pore size filter and acidified using HNO_3. The Pb(II) concentration in these samples was then determined by graphite furnace atomic absorption spectrometry (GFAAS, Agilent Z240, U.S.A.).

Results and discussion

Reactive surface structure of the activated carbon

DFT calculations. DFT calculations were carried to investigate the interaction between Pb(II) and AC.

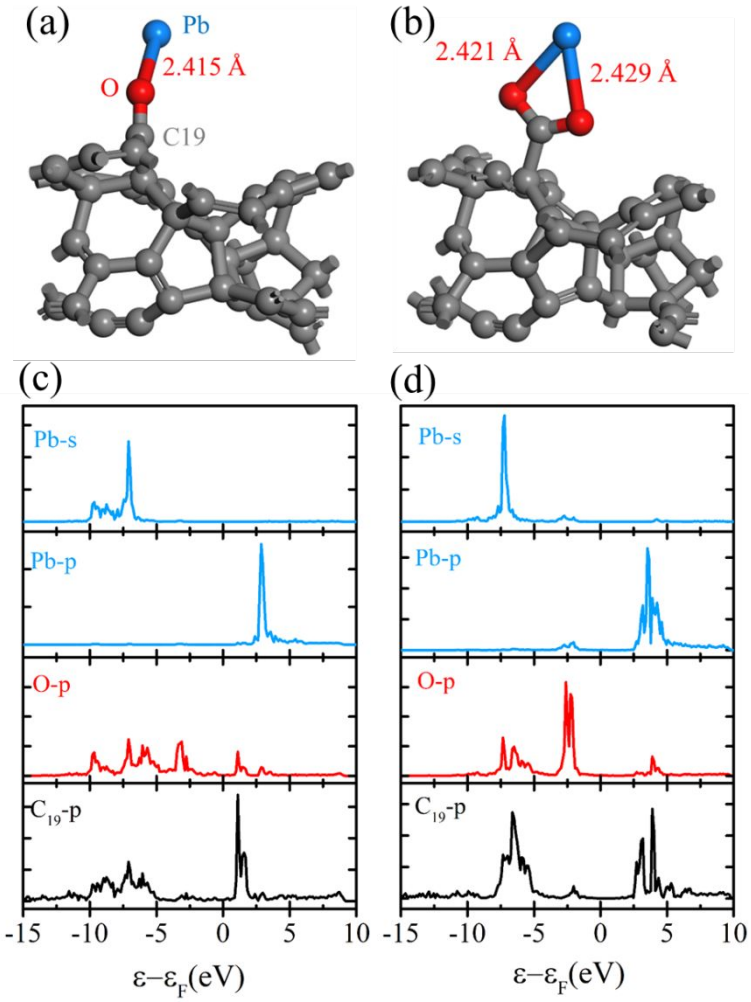

Figure 1. DFT geometry-optimized structure for Pb(II) complexed with phenol (a) and carboxyl (b) groups on AC surface and corresponding (c) and (d) PDOS analysis results of *p* orbitals of C_{19}, O, and Pb, and *s* orbital of Pb. The value of the Fermi energy (ε_F) was set at x = 0.

A single carboxyl group or phenol group was placed on the C_{19} position (Figure S2), corresponding to a functional group density of approximately 1.7 site/nm^2, selected on the basis of the reported active adsorption site density of AC, which is between 0.05 and 2.6 site/nm^2 [47-49]. After geometry optimization, the carboxyl group complexed C_{19} atom was separated from the carbon bulk due to the attraction of two oxygen atoms. This behavior is

in agreement with previous observation for Pb(II) adsorption onto carbon nanotubes [13].

The optimized surface was then used to study the adsorption of Pb(II). The atom was placed on the AC surface to investigate the interaction between Pb(II) and the two functional groups as shown in Figure S2a and b in the SI document. Upon surface geometry optimization, the Pb(II) was found to be attracted by oxygen atoms on the AC surface and the optimized distances between Pb(II) and O atoms ($r_{Pb\text{-}O}$) of phenol and carboxyl groups were 2.415 Å, and 2.421 and 2.429 Å, respectively (Figure 1a and b). These results are in agreement with the values reported in previous DFT calculations for Pb(II) adsorption on carbon nanotube and graphene oxides[13-15]. The adsorbed Pb(II) on the carboxyl group of the AC surface was always chelated by the two oxygen atoms of the carboxyl group, independent on the initial position of Pb(II) placed (Figure S3).

Partial density of state (PDOS) analysis was carried out to investigate the contributions of the *s*, *p*, or *d* orbitals of the participating atoms, including Pb, O, and the complexed carbon atoms (C_{19}, Figure 1c and d). The PDOS analysis of the Pb(II)-complexed phenol group clearly showed overlapping peaks around -7.1 eV of Pb-*s,* O-*p*, and C_{19}-*p* (Figure 1c). On the other hand, for Pb(II) complexed with the carboxyl group, the PDOS analysis showed overlapping peaks around -7.2 eV of Pb-*s,* O-*p,* and C-*p*, and -2.2 to -2.8 eV between Pb-*p,* O-*p,* and C_{19}-*p* (Figure 1d). These overlapping peaks indicate a covalent interaction between Pb(II) and O, which is caused by the hybridizations of the *s* and *p* orbitals from Pb(II) and the *p* orbital from O. These results are in agreement with the

experimental observations by Bargar *et al.*[19]. Moreover, the Pb-*p* orbital shows no significant overlapping peaks when Pb(II) complexed with phenol group, which implies a binding interaction between Pb(II) and phenol which is weaker than between Pb(II) and the carboxyl group. Moreover, the overlapping peaks of the Pb -s and -p, O-p, and C_{19}-p orbitals on the similar occupied energies implied the effect of Pb-O bond on the interaction between C_{19} and O.

The adsorption energy was also calculated, and the details are described in the SI. As shown in Table S1 and S2, the adsorption energies for Pb(II) adsorption on the carboxyl and phenol groups are 278.495 and -124.943 kJ/mol, respectively. The results suggested that the adsorption of Pb(II) on protonated carboxyl group is an endergonic process as the calculated energy (278.495 kJ/mol) is positive, which did not agree with our experimental results and the previous work[15]. However, the carboxyl group is usually deprotonated at pH > 4, based on its reported pk_a values (2.68~4.0)[50, 51]. Therefore, the adsorption of the Pb(II) on the deprotonated carboxyl group (=COO^-) was also calculated (-288.588 kJ/mol), which indicated a spontaneous exergonic process of adsorption of Pb(II) on the deprotonated carboxyl group. Possible adsorption on both protonated and deprotonated carboxyl groups have been reported in the literature[45, 52, 53]. However, the results reported here show that the reaction with the latter type of site is more favorable.

Experimental validation. To validate these calculations, pellet-FTIR and XAS analyses were performed. The samples were prepared using Sol 1 and 2, as explained in the section

of Pellet-FTIR analysis. The measured spectra show well-resolved peaks between 850 and 1700 cm^{-1} (Figure 2), which result from the IR vibrations of functional groups on the AC surface, usually including carboxyl, phenol, ether, and C-H groups. As these IR vibrations give overlapping peaks, the locations of the modes of vibrations were identified on the basis of the second-order derivative (Figure S4 and Table S3).

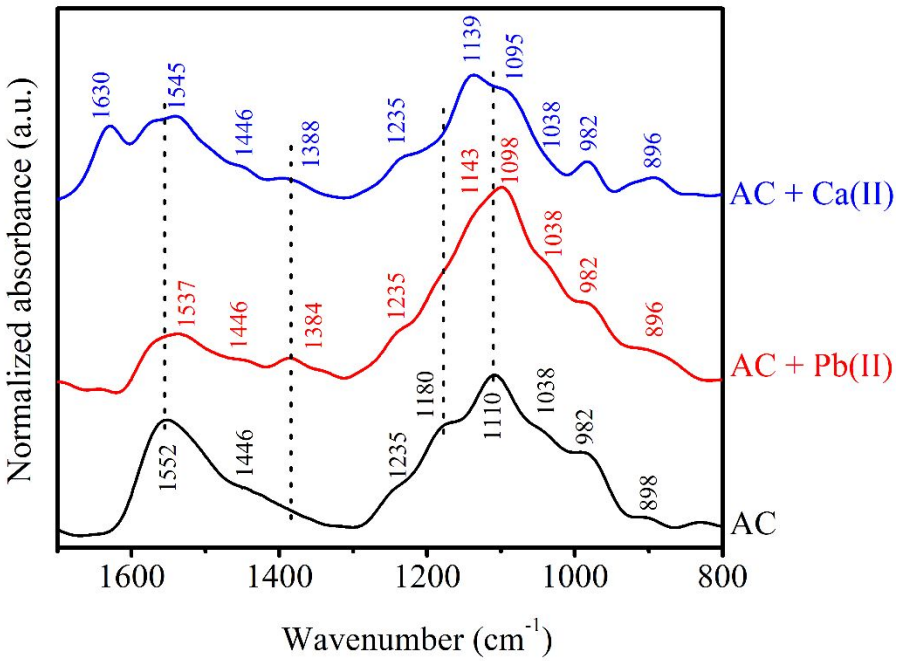

Figure 2. Pellet-FTIR analysis results showing the FTIR spectra of for various AC surfaces. Dashed lines highlight the shifts in vibration modes. The composition of the solutions was: AC = 0.1 g/L, ionic strength = 0.01 M NaCl, Pb(II) = 1 mg/L, Ca(II) = 50 mg/L, and pH = 5.0 ± 0.2.

Peaks between 1350 and 1600 cm^{-1} for AC correspond to the carboxyl group stretching vibrations, while at 1552 and 1446 cm^{-1}, the peaks are due to the asymmetric and symmetric stretch of COO^-, respectively[54-58]. The overlapped peaks between 850 and 1300 cm^{-1} result from C-O stretching, namely: the asymmetric stretch of the C-O-C group at 1235 cm^{-1} [59-62], the symmetric stretch of C-O-C at 1038 cm^{-1} [62, 63], the asymmetric stretch of C-O-H at

1180 cm^{-1}, and the symmetric stretch of C-O-H at 1110 cm^{-1} [64, 65]. Additionally, the peaks at 982 and 898 cm^{-1} result from in-plane and out-of-plane C-H bending, respectively[64, 66].

Upon adsorption of Pb(II) onto AC, the position of the highest intensity peak among the carboxyl group IR bands shifted from 1552 to 1537 cm^{-1}, and a new peak appeared at 1384 cm^{-1}. This was due to the asymmetric and symmetric stretches of COO^- complexed with Pb(II) [55, 57, 58]. Similarly, the peaks at 1180 and 1110 cm^{-1} also decreased to 1143 and 1098 cm^{-1}, respectively, because of the complexation of the COH surface group on AC with Pb(II). In addition, peaks at 1235, 1038, 982, and 898 cm^{-1} had no significant shift after Pb(II) adsorption, indicating that the ether and the C-H groups on AC did not form any complex with Pb(II).

In order to investigate the local coordination environment of Pb(II) upon adsorption onto AC, XAS analysis was carried out (Figure 3 and Table S4). The sample was prepared using Sol 2, as explained in the section of XAS analysis. As shown in Figure 3b, the first Fourier transform (FT) peak observed in the Pb-L_{III} edge EXAFS spectrum was described by 1.3 oxygen atoms with a distance of 2.32 Å. The interatomic distance between Pb(II) and oxygen agrees well with previous results for Pb(II) adsorption on metal oxides[19, 20, 67, 68], within 0.1 Å error compared to our DFT calculation (2.415-2.429 Å). A coordination number (CN) of 1.3 was caused by one and two oxygens from phenol and carboxyl groups, respectively. This CN larger than 1 is due to a strong backscattering of C atoms. Moreover, an additional peak from 0.4 carbon atoms at 3.12 Å provides a CN less than 1, which is due to a weak backscattering of C atoms, instead.

These results confirm that Pb(II) strongly reacts with phenol and carboxyl groups on the AC surface forming mononuclear complexes.

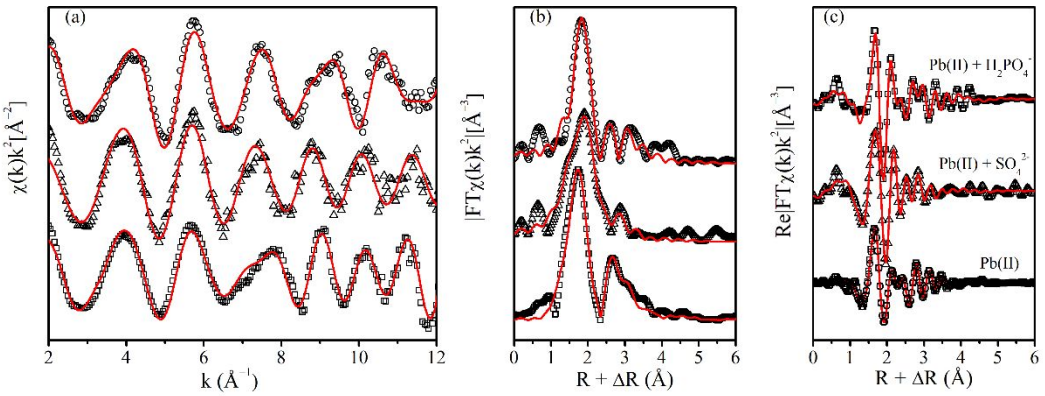

Figure 3. XAS analysis results of Pb(II) adsorption on AC surface. (a) Normalized k^2-weighted experimental (symbols) and fitted (lines) Pb L_{III}-edge EXAFS spectra of Pb(II) adsorption on AC at pH 5 in the absence (squares) and presence of SO_4^{2-} (triangles) and $H_2PO_4^-$ (circles). (b) Corresponding Fourier transformed magnitude. (c) Real parts of the Fourier transform.

Competitive adsorption between Pb(II) and Ca(II) on the AC surface

Among the common cations in tap water (i.e. sodium (Na(I)), magnesium (Mg(II)), and Ca(II)), Ca(II) showed more significant competitive effect on Pb(II) removal by AC than Mg(II) and Na(I) (Figure S5). Therefore, upon the determination of the surface structure of AC in the presence of Pb(II), the change of the surface geometry due the presence of Ca(II) was investigated experimentally through pellet-FTIR and XAS analysis. The sample was prepared using Sol 1 and 3, as explained in the section of XAS analysis. The FTIR results, reported in Figure 2 and Table S3, show a significant shift of IR peaks after adsorption of Ca(II) onto the AC surface, as in the case of Pb(II). Namely, a shift of the asymmetric and symmetric stretches of COO^- from 1552 to 1545 cm^{-1}, and 1446 to

1388 cm^{-1}, respectively, was observed. This suggests a complexation of Ca(II) with the carboxyl groups of the AC surface. The shift of peaks from 1180 to 1139 cm^{-1} and 1110 to 1095 cm^{-1} indicate changes in the asymmetric and symmetric stretches, suggesting also a complexation of Ca(II) with the phenol groups. Moreover, the O-H bending from H_2O molecules was observed significantly at 1630 cm^{-1} after Ca(II) adsorption[69, 70]. This is because of the hydration shell of Ca(II), which can contain up to 8 molecules[71, 72].

The fitting of the K-edge EXAFS spectrum for Ca(II) adsorption onto AC shows four shells (Figure 4, Table S5). The first shell was ascribed to 1.9 O atoms at 2.01 Å, which is due to the complexation of Ca(II) with carboxyl and phenol groups on the AC surface. The second shell was associated to 1 O atom at 2.49 Å resulting from the waters of hydration surrounding Ca(II) [73-75]. Moreover, two shells of C atoms were detected at 3.11 and 4.06 Å, which correspond to the interatomic distances between C and Ca(II) ($r_{Ca\text{-}C}$) for the formation of inner- and outer-sphere complexes, respectively, upon Ca(II) adsorption onto the AC surface.

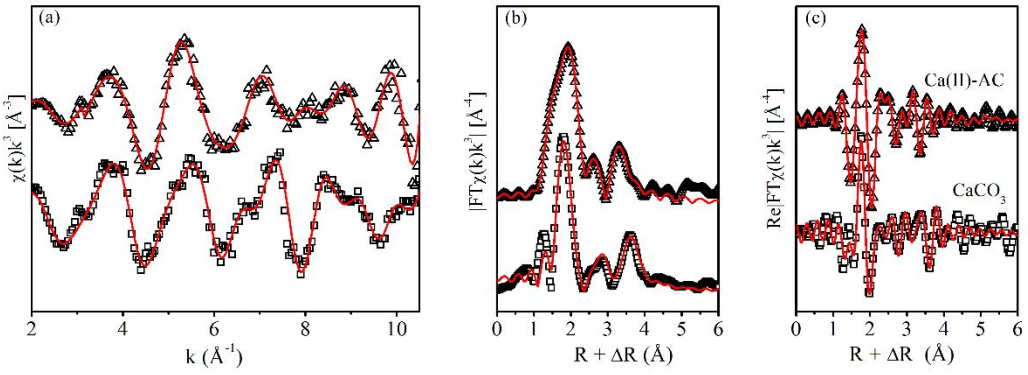

Figure 4. XAS analysis results of Ca(II) adsorption on AC surface. (a) Normalized k^3-weighted experimental (symbols) and fitted (lines) Ca K-edge EXAFS spectra of $CaCO_3$

(squares) and Ca(II) adsorption on AC (triangles) at pH 5. (b) Corresponding Fourier transformed magnitude. (c) Real parts of the Fourier transform.

These results confirm that Ca(II) can indeed strongly react with phenol and carboxyl groups on the AC surface, competing therefore with Pb(II) for adsorption on these sites.

Effect of SO_4^{2-} on Pb(II) adsorption

EXAFS spectra of Pb(II) adsorption onto AC with SO_4^{2-} were analyzed to explore the interaction between Pb(II) and SO_4^{2-} on the AC surface (Figure 3 and Table S4). The sample was prepared using Sol 5, as explained in the section of XAS analysis. In the presence of SO_4^{2-}, the CN of the first O shell surrounding Pb(II) increased from 1.3 to 2.7, indicating the complexation of Pb(II) with the O in the SO_4^{2-} ion. Moreover, the formation of this complex resulted in a second O shell at 2.72 Å with a CN of 0.7. *In situ* flow cell ATR-FTIR technique was also used to investigate the changes in the coordination of SO_4^{2-} on the AC surface (Figure 5 and S6), as performed in previous works to study SO_4^{2-} adsorption onto goethite[21, 76, 77]. The samples in this work were prepared using Sol 4 and 5, as explained in the section of XAS analysis and the results are reported in Figure 5. The figure shows a single peak centered at 1104 cm^{-1}, which is characteristic of a triply degenerate asymmetric stretching (v_3) band of S-O in un-protonated tetrahedral SO_4^{2-}, confirming that the tetrahedral dissolved SO_4^{2-} ion is un-protonated (T_d symmetry), at the investigated conditions, i.e., pH 5. Upon adsorption of SO_4^{2-} onto AC, two broad bands appear at 1110 and 965 cm^{-1}, corresponding to v_3 and v_1 (symmetric stretching of S-O) vibrations. Broad peaks usually have been attributed to outer-sphere adsorbed SO_4^{2-} [21, 26,

[76, 78]. However, the peak here in the v_3 region shows two weak shoulders, which could be fitted by three modes at 1168, 1112, and 1079 cm^{-1}, suggesting a C_{2v} symmetry for adsorbed SO_4^{2-} on AC. The C_{2v} symmetry corresponds to bidentate mononuclear or bidentate binuclear un-protonated adsorbed SO_4^{2-}, which partially exists on the AC surface.

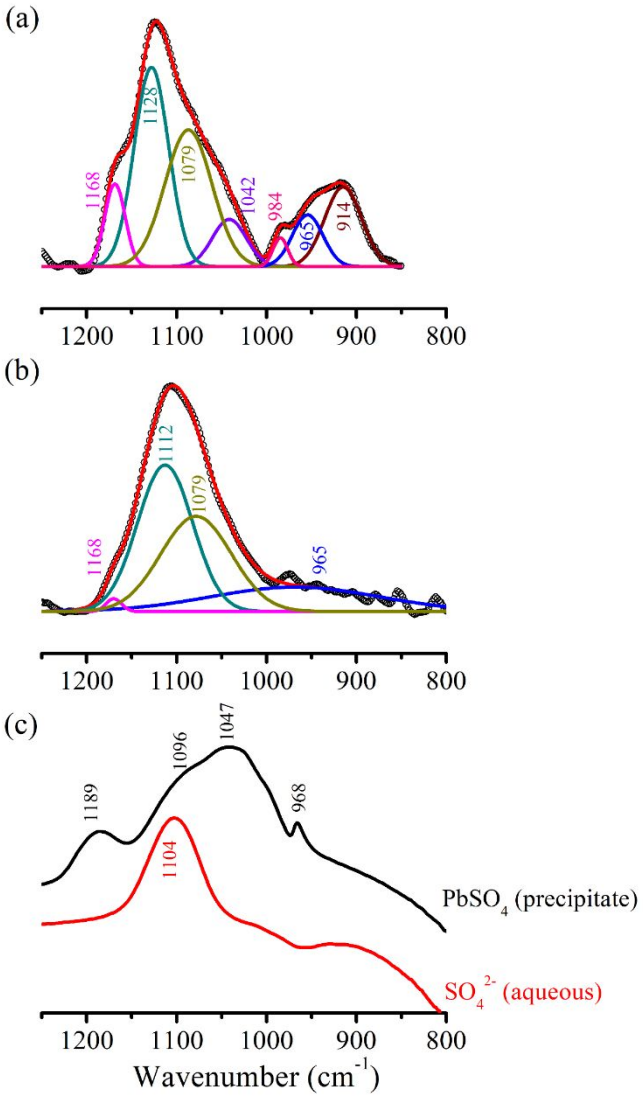

Figure 5. *In situ* flow cell ATR-FTIR spectra. (a) Data (open circles) and fitting (red line) for 30 mg/L SO_4^{2-} adsorption on AC in the presence and (b) absence of 1 mg/L Pb(II). (c) ATR-FTIR spectra of dissolved 0.1 M SO_4^{2-} and $PbSO_4$ precipitate in solution at pH 5.

Fitting the IR spectrum of adsorbed SO_4^{2-} on AC in the presence of Pb(II) yields seven modes in the v_3 and v_1 regions. These modes are different from those of precipitate of lead phosphate ($PbSO_4$), indicating that no precipitate was formed. The band number of seven indicated that more than one symmetric structure of adsorbed inner-sphere SO_4^{2-} was formed, suggesting that complexation took place between SO_4^{2-} and Pb(II) adsorbed onto AC. Moreover, the outer-sphere adsorbed SO_4^{2-} also complexed with Pb(II), as can be seen from the significant shift of the IR mode from 1112 to 1128 cm^{-1} and the presence of an additional O atom at 2.72 Å in the EXAFS results.

These measurements show that SO_4^{2-} ions could form complexes with Pb(II) on the AC surfaces, which enhanced Pb(II) adsorption.

Effect of $H_2PO_4^-$ on Pb(II) adsorption

EXAFS spectra of Pb(II) adsorption onto AC with $H_2PO_4^-$ were analyzed to explore the interaction between Pb(II) and $H_2PO_4^-$ on the AC surface (Figure 3 and Table S4). The sample was prepared using Sol 7, as explained in the section of XAS analysis. Results from the fitting of the Pb L_{III}-edge EXAFS spectrum indicates the presence of 1.3 O atoms at 2.33 Å and of 0.6 C atoms at 3.08 Å (Table S4) indicating no significant change from those in the absence of $H_2PO_4^-$. A second peak was observed, and it was described using an additional C shell at 3.62 Å with CN of 0.4. To clarify if this shell resulted from the formation of pyromorphite ($Pb_5(PO_4)_3Cl$, log k =79.6[79]), Pb-Pb path was also used to fit the third FT peak. Results in Figure S7 show that the third FT peak fitting using Pb-C path

(R-factor = 0.28, Table S4) is better than that using Pb-Pb path (R-factor = 0.31).

The EXAFS results suggest the formation of a surface ternary complex between Pb(II) and $H_2PO_4^-$ on AC rather than the precipitate of $Pb_5(PO_4)_3Cl$. To confirm this finding, transmission electron microscopy (TEM) was also employed to monitor the precipitate formed in the solution in the absence and presence of AC (Figure S8). From these measurements, it is obvious that precipitates formed in the presence of AC have a smaller amount and particle size than that formed without AC. This difference was further evidenced by the selected area electron diffraction (SAED) characterization. Most of the diffraction spots of $Pb_5(PO_4)_3Cl$ (Figure S8-b) disappeared for the precipitate formed in the presence of AC (Figure S8-c). The poorer crystalline $Pb_5(PO_4)_3Cl$ implied the formation of this mineral was inhibited due to the presence of AC, which agreed well with our EXAFS results. Similar with our results, Xie *et al.* [80] studied Pb(II) adsorption onto iron oxides in the presence of $H_2PO_4^-$, in which adsorption dominated the adsorption process rather than formation of a precipitate.

The *in situ* flow cell ATR-FTIR technique was also used to analyze the interaction between $H_2PO_4^-$ and Pb(II) on the AC surface (Figure 7 and S6). The samples were prepared using Sol 6 and 7, as explained in the section of XAS analysis. At pH 5, $H_2PO_4^-$ in solution is double-protonated (C_{2v} symmetry), resulting in four modes at 1156, 1075, 938, and 873 cm^{-1}. Adsorbed $H_2PO_4^-$ on the AC surface shows a broad peak, which is significantly different from the spectrum of dissolved $H_2PO_4^-$. This broad peak could be

fitted by four modes at 1115, 1074, 1038, and 961 cm^{-1}, suggesting a C_{2v} symmetric structure for $H_2PO_4^-$ adsorption on AC. The C_{2v} symmetry for adsorbed $H_2PO_4^-$ on the ferrihydrite surface was reported in a previous study [81], which suggested an un-protonated bidentate binuclear complex. In this study, the protonation status of $H_2PO_4^-$ on the AC surface was not investigated. Thus, the C_{2v} symmetric structure for $H_2PO_4^-$ on the AC surface could be attributed to either an un- or doubly-protonated bidentate configuration.

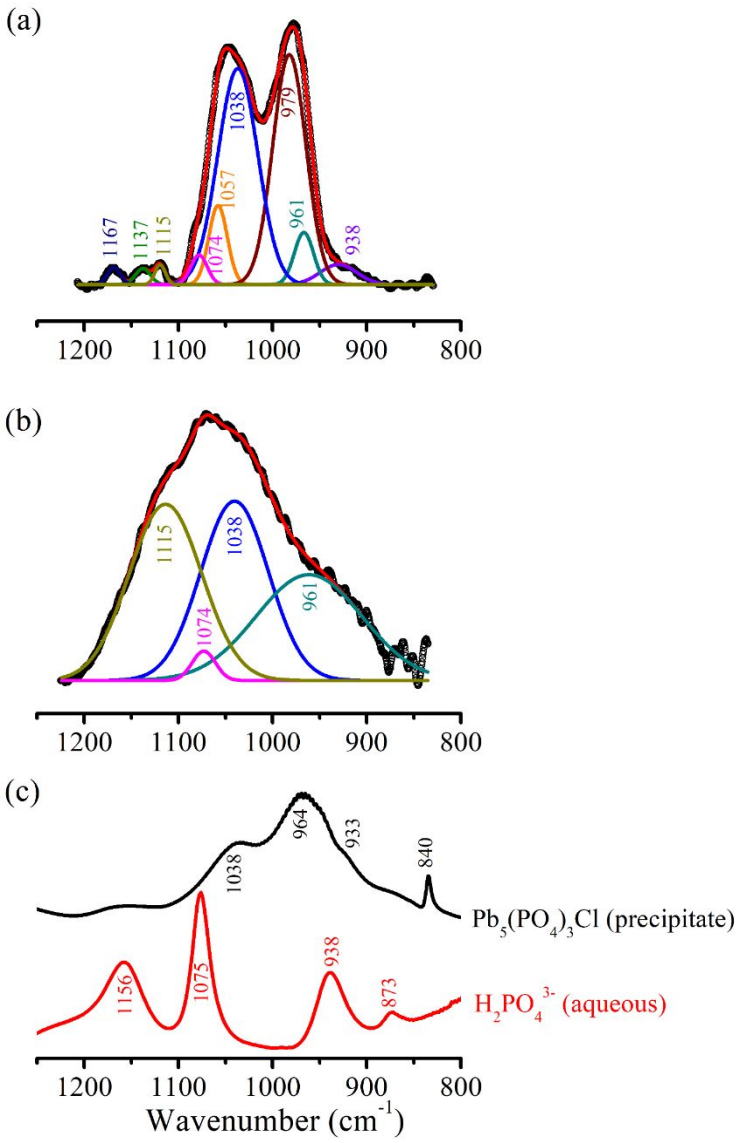

Figure 6. *In situ* flow cell ATR-FTIR spectra. (a) Data (open circles) and fitting (red line) for 1 mg/L $H_2PO_4^-$ (as P) adsorption on AC in the presence and (b) the absence of 1 mg/L Pb(II). (c) ATR-FTIR spectra of dissolved 0.1 M $H_2PO_4^-$ and $Pb(PO_4)_3Cl$ precipitate in solution at pH 5.

The presence of Pb(II) caused a significant change in the IR spectrum for $H_2PO_4^-$ adsorbed on AC. Nine IR bands were resolved by curve fitting, indicating the presence of more than one symmetric complex on the AC surface. Therefore, similar to SO_4^{2-}, $H_2PO_4^-$ could form a surface ternary complex with Pb(II) on the AC surface.

Results from the EXAFS and *in situ* ATR-FTIR analyses suggest that $H_2PO_4^-$ and Pb(II) ions prefer to form ternary complexes on the AC surface rather than forming precipitate in solution.

Surface complexation model based on molecular observations

Based on the DFT calculated structures and spectroscopic results for Pb(II) adsorption on AC under various conditions, as well as the spectroscopic results for Ca(II) adsorption on AC, a surface complexation model was developed and applied to simulate the experimental results of batch tests. The major chemical reactions write as,

$$COO^{-1/2} + Pb^{2+} = COOPb^{+3/2} \quad \textbf{(1)}$$

$$CO^{-1/2} + Pb^{2+} = COPb^{+3/2} \quad \textbf{(2)}$$

$$COO^{-1/2} + Ca^{2+} = COOCa^{+3/2} \quad \textbf{(3)}$$

$$CO^{-1/2} + Ca^{2+} = COCa^{+3/2} \quad \textbf{(4)}$$

$$COO^{-1/2} + Pb^{2+} + SO_4^{2-} = COOPbSO_4^{-1/2} \quad \textbf{(5)}$$

$$CO^{-1/2} + Pb^{2+} + SO_4^{2-} = COPbSO_4^{-1/2} \quad \textbf{(6)}$$

$$COO^{-1/2} + Pb^{2+} + PO_4^{3-} + 2H^+ = COOPbH_2PO_4^{1/2} \quad \textbf{(7)}$$

$$CO^{-1/2} + Pb^{2+} + PO_4^{3-} + 2H^+ = COPbH_2PO_4^{1/2} \quad \textbf{(8)}$$

where reactions 1 and 2 describe the adsorption of Pb(II) on carboxyl and phenol groups on AC as observed in the DFT calculations and spectroscopic measurements (section: Reactive surface structure of the activated carbon); reactions 3 and 4 describe the adsorption of Ca(II), as observed in the spectroscopic measurements (section: Competitive adsorption between Pb(II) and Ca(II) on the AC surface); and reactions 5 through 8 describe the formation of ternary surface complex for Pb(II) adsorption on AC in the presence of SO_4^{2-} and $H_2PO_4^-$ ions, as observed in the spectroscopic measurements (sections: Effect of SO_4^{2-} on Pb(II) adsorption and Effect of $H_2PO_4^-$ on Pb(II) adsorption).

These reactions were then implemented using a surface complex model of charge distribution multisite ion complexation (CD-MUSIC) (Table S6). The measurements of adsorption performed as described in the section of Batch experiment are shown in Figure 7 with the chemical model upon fitting.

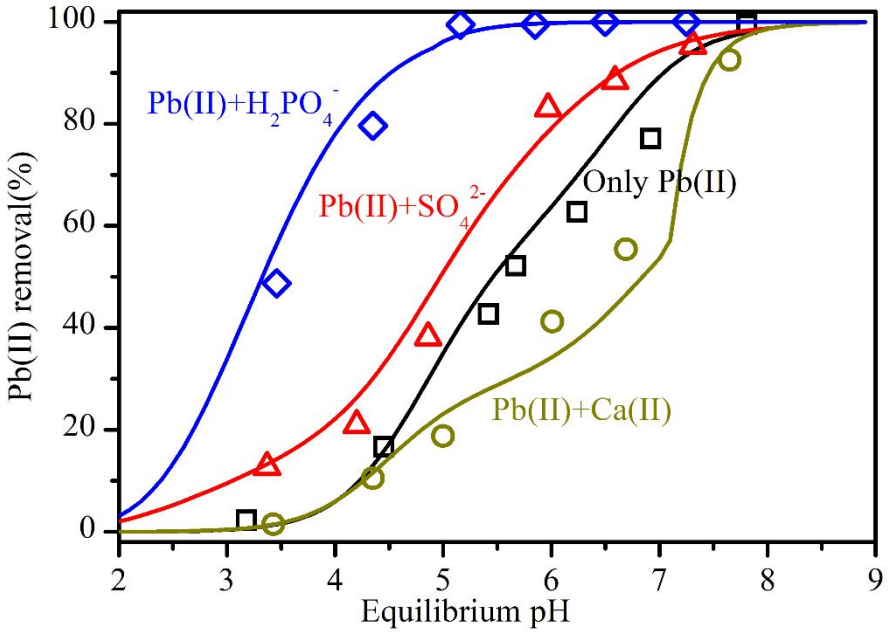

Figure 7. Measurements and model of the adsorption of Pb(II) on AC as a function of pH, data are shown with symbols and the model is given with continuous lines. Namely, Only Pb(II) (black squares), Pb(II) and Ca(II) (dark yellow circles), Pb(II) and SO_4^{2-} (red triangles), and Pb(II) and $H_2PO_4^-$ (blue diamonds). (Ionic strength = 0.01 M NaCl, adsorbent dose = 0.1 g/L, adsorption time = 4 h, SO_4^{2-} = 30 mg/L, $H_2PO_4^-$-P = 1 mg/L).

As shown in Figure 7, the model can describe very well the measurements. The fraction of different Pb(II) species were shown in Figure S9. It is obvious that Pb(II) prefers to complex with carboxyl rather than phenol group on AC at pH 3-8 (Figure S9-a), which is in agreement with DFT calculations. The results show that the presence of Ca(II) reduces Pb(II) adsorption, confirming the competitive adsorption of Pb(II) and Ca(II) on AC (Figure S9-b). On the contrary, SO_4^{2-} and $H_2PO_4^-$ enhanced Pb(II) removal by AC by forming surface ternary complexes (Figure S9-c and d), resulting in the experimental phenomenon of the promotion of Pb(II) removal at pH 3.2-6.8. The surface complexation model predicts that, in the presence of $H_2PO_4^-$, the amount of $Pb_5(PO_4)_3Cl$ in solid form at pH 5 is 9.0% (Figure S9-d). This value is much lower than amount of AC-Pb(II)-PO_4 ternary complex (79.7%), suggesting that the ternary surface complexation dominate Pb(II) removal, agreed well with our EXAFS and *in situ* ATR-FTIR measurements.

Conclusions

A mechanistic study based on the combination of DFT calculations and various spectroscopic analyses was carried out to understand the adsorption of Pb(II) onto AC surface and potentially other carbonaceous materials. The results revealed the formation of monodentate Pb(II)-phenol and bidentate Pb(II)-carboxyl, as well as the formation of ternary AC-Pb(II)-SO_4 and AC-Pb(II)-PO_4 complexes on AC surfaces. Moreover, this

work confirmed a competitive adsorption behavior between Pb(II) and Ca(II) onto AC and instead a synergetic behavior between Pb(II) and SO_4^{2-} and $H_2PO_4^-$ ions. These results allowed to formulate chemical reactions of Pb(II) with carboxyl and phenol groups on the AC surface in the presence of co-existing ions and develop a surface complexation model. The model agrees very well with measurements performed in batch. Therefore, it is valuable tool to describe the behavior of Pb(II) in the presence of AC and to improve the design of filters employing AC-based materials.

ACKNOWLEDGEMENTS

This research used resources of the Advanced Photon Source, a U.S. Department of Energy (DOE) Office of Science User Facility operated for the DOE Office of Science by Argonne National Laboratory under Contract No. DE-AC02-06CH11357. The Extreme Science and Engineering Discovery Environment (XSEDE), which is supported by National Science Foundation Grant OCI-1053575, supplied computational time for our study.

Supporting information available: Figures and Tables of effect from co-existing Na(I), Mg(II), and Ca(II), FTIR analysis, EXAFS collecting and fitting procedures, DFT calculations, surface complex modeling. This material is available online at https://pubs.acs.org.

References:

(1) Edwards, M.; Dudi, A., role of chlorine and chloramine in corrosion of lead-bearing plumbing materials. *Journal (American Water Works Association)* **2004,** *96*, 69-81.

(2) McNeill, L. S.; Edwards, M., Importance of Pb and Cu Particulate Species for Corrosion Control. *J. Environ. Eng.* **2004,** *130*, 136-144.

(3) Nordberg, G. F.; Fowler, B. A.; Nordberg, M., *Handbook on the Toxicology of Metals*. Academic Press: 2014.

(4) Edwards, M.; Triantafyllidou, S.; Best, D., Elevated Blood Lead in Young Children Due to Lead-Contaminated Drinking Water: Washington, DC, 2001−2004. *Environ. Sci. Technol.* **2009,** *43*, 1618-1623.

(5) Kadirvelu, K.; Thamaraiselvi, K.; Namasivayam, C., Removal of heavy metals from industrial wastewaters by adsorption onto activated carbon prepared from an agricultural solid waste. *Bioresour. Technol.* **2001,** *76*, 63-65.

(6) Wang, L.; Zhang, J.; Zhao, R.; Li, Y.; Li, C.; Zhang, C. L., Adsorption of Pb(II) on activated carbon prepared from Polygonum orientale Linn.: Kinetics, isotherms, pH, and ionic strength studies. *Bioresour. Technol.* **2010,** *101*, 5808-5814.

(7) Dwivedi, C. P.; Sahu, J. N.; Mohanty, C. R.; Mohan, B. R.; Meikap, B. C., Column performance of granular activated carbon packed bed for Pb(II) removal. *J. Hazard. Mater.* **2008,** *156*, 596-603.

(8) Mouni, L.; Merabet, D.; Bouzaza, A.; Belkhiri, L., Adsorption of Pb(II) from aqueous solutions using activated carbon developed from Apricot stone. *Desalination* **2011,** *276*, 148-153.

(9) Kadirvelu, K.; Faur-Brasquet, C.; Le Cloirec, P., Removal of Cu(II), Pb(II), and Ni(II) by adsorption onto activated carbon cloths. *Langmuir* **2000,** *16*, 8404-8409.

(10) Swiatkowski, A.; Pakula, M.; Biniak, S.; Walczyk, M., Influence of the surface chemistry of modified activated carbon on its electrochemical behaviour in the presence of lead(II) ions. *Carbon* **2004,** *42*, 3057-3069.

(11) Ho, Y.-S.; Ofomaja, A. E., Effects of calcium competition on lead sorption by palm kernel fibre. *J. Hazard. Mater.* **2005,** *120*, 157-162.

(12) Shi, Q.; Terracciano, A.; Zhao, Y.; Wei, C.; Christodoulatos, C.; Meng, X., Evaluation of metal oxides and activated carbon for lead removal: Kinetics, isotherms, column tests, and the role of co-existing ions. *Sci. Total Environ.* **2019,** *648*, 176-183.

(13) Bastos, M.; Camps, I., Interactions of lead with carboxyl and hydroxyl-decorated(10, 0) single-walled carbon nanotubes: First-principle calculations. *Appl. Surf. Sci.* **2013,** *285, Part B*, 198-204.

(14) Yang, S. B.; Chen, C. L.; Chen, Y.; Li, J. X.; Wang, D. Q.; Wang, X. K.; Hu, W. P., Competitive Adsorption of Pb-II, Ni-II, and Sr-II Ions on Graphene Oxides: A Combined Experimental and Theoretical Study. *Chempluschem* **2015,** *80*, 480-484.

(15) Saleh, T. A.; Gupta, V. K.; Al-Saadi, A. A., Adsorption of lead ions from aqueous solution using porous carbon derived from rubber tires: Experimental and computational study. *J. Colloid Interface Sci.* **2013,** *396*, 264-269.

(16) Wang, X. X.; Chen, Z. S.; Yang, S. B., Application of graphene oxides for the removal of Pb(II) ions from aqueous solutions: Experimental and DFT calculation. *J. Mol. Liq.* **2015,** *211*, 957-964.

(17) Mason, S. E.; Iceman, C. R.; Tanwar, K. S.; Trainor, T. P.; Chaka, A. M., Pb(II) Adsorption on Isostructural Hydrated Alumina and Hematite (0001) Surfaces: A DFT Study. *J. Phys. Chem. C* **2009,** *113*,

2159-2170.

(18) Mason, S. E.; Trainor, T. P.; Chaka, A. M., Hybridization-reactivity relationship in Pb(II) adsorption on α-Al2O3-water interfaces: A DFT Study. *J. Phys. Chem. C* **2011,** *115*, 4008-4021.

(19) Bargar, J. R.; Brown, G. E.; Parks, G. A., Surface complexation of Pb(II) at oxide-water interfaces: I. XAFS and bond-valence determination of mononuclear and polynuclear Pb(II) sorption products on aluminum oxides. *Geochim. Cosmochim. Acta* **1997,** *61*, 2617-2637.

(20) Bargar, J. R.; Brown, G. E.; Parks, G. A., Surface complexation of Pb(II) at oxide-water interfaces: II. XAFS and bond-valence determination of mononuclear Pb(II) sorption products and surface functional groups on iron oxides. *Geochim. Cosmochim. Acta* **1997,** *61*, 2639-2652.

(21) Elzinga, E. J.; Peak, D.; Sparks, D. L., Spectroscopic studies of Pb(II)-sulfate interactions at the goethite-water interface. *Geochim. Cosmochim. Acta* **2001,** *65*, 2219-2230.

(22) Matocha, C. J.; Elzinga, E. J.; Sparks, D. L., Reactivity of Pb(II) at the Mn(III,IV) (Oxyhydr)Oxide−Water Interface. *Environ. Sci. Technol.* **2001,** *35*, 2967-2972.

(23) Beattie, D. A.; Chapelet, J. K.; Gräfe, M.; Skinner, W. M.; Smith, E., In Situ ATR FTIR Studies of SO4 Adsorption on Goethite in the Presence of Copper Ions. *Environ. Sci. Technol.* **2008,** *42*, 9191-9196.

(24) Fang, L.; Shi, Q.; Nguyen, J.; Wu, B.; Wang, Z.; Lo, I. M. C., Removal Mechanisms of Phosphate by Lanthanum Hydroxide Nanorods: Investigations using EXAFS, ATR-FTIR, DFT, and Surface Complexation Modeling Approaches. *Environ. Sci. Technol.* **2017,** *51*, 12377-12384.

(25) Flynn, E. D.; Catalano, J. G., Competitive and Cooperative Effects during Nickel Adsorption to Iron Oxides in the Presence of Oxalate. *Environ. Sci. Technol.* **2017,** *51*, 9792-9799.

(26) Ostergren, J. D.; Brown, G. E.; Parks, G. A.; Persson, P., Inorganic ligand effects on Pb(II) sorption to goethite (alpha-FeOOH) - II. Sulfate. *J. Colloid Interface Sci.* **2000,** *225*, 483-493.

(27) Ostergren, J. D.; Brown, G. E.; Parks, G. A.; Persson, P., Inorganic Ligand Effects on Pb(II) Sorption to Goethite (α-FeOOH). *J. Colloid Interface Sci.* **2000,** *225*, 483-493.

(28) Kresse, G.; Furthmüller, J., Efficiency of ab-initio total energy calculations for metals and semiconductors using a plane-wave basis set. *Comput. Mater. Sci.* **1996,** *6*, 15-50.

(29) Perdew, J. P.; Burke, K.; Ernzerhof, M., Generalized gradient approximation made simple. *Phys. Rev. Lett.* **1996,** *77*, 3865-3868.

(30) Blöchl, P. E., Projector augmented-wave method. *Phys. Rev. B* **1994,** *50*, 17953-17979.

(31) Kresse, G.; Joubert, D., From ultrasoft pseudopotentials to the projector augmented-wave method. *Phys. Rev. B* **1999,** *59*, 1758-1775.

(32) Monkhorst, H. J.; Pack, J. D., Special Points for Brillouin-Zone Integrations. *Phys. Rev. B* **1976,** *13*, 5188-5192.

(33) Mathew, K.; Sundararaman, R.; Letchworth-Weaver, K.; Arias, T.; Hennig, R. G., Implicit solvation model for density-functional study of nanocrystal surfaces and reaction pathways. *The Journal of chemical physics* **2014,** *140*, 084106.

(34) Fishman, M.; Zhuang, H. L.; Mathew, K.; Dirschka, W.; Hennig, R. G., Accuracy of exchange-correlation functionals and effect of solvation on the surface energy of copper. *Phys. Rev. B* **2013,** *87*, 245402.

(35) Grimme, S.; Antony, J.; Ehrlich, S.; Krieg, H., A consistent and accurate ab initio parametrization of density functional dispersion correction (DFT-D) for the 94 elements H-Pu. *The Journal of chemical physics* **2010,** *132*, 154104.

(36) Grimme, S.; Ehrlich, S.; Goerigk, L., Effect of the damping function in dispersion corrected density functional theory. *J. Comput. Chem.* **2011,** *32*, 1456-1465.
(37) Harris, P. J. F.; Liu, Z.; Suenaga, K., Imaging the atomic structure of activated carbon. *Journal of Physics-Condensed Matter* **2008,** *20*.
(38) Zhao, J.; Yang, L.; Li, F.; Yu, R.; Jin, C., Structural evolution in the graphitization process of activated carbon by high-pressure sintering. *Carbon* **2009,** *47*, 744-751.
(39) Newville, M., IFEFFIT: interactive XAFS analysis and FEFF fitting. *J. Synchrotron Radiat.* **2001,** *8*, 322-324.
(40) Ravel, B.; Newville, M., ATHENA, ARTEMIS, HEPHAESTUS: data analysis for X-ray absorption spectroscopy using IFEFFIT. *J. Synchrotron Radiat.* **2005,** *12*, 537-541.
(41) Shi, Q. T.; Yan, L.; Chan, T. S.; Jing, C. Y., Arsenic Adsorption on Lanthanum-Impregnated Activated Alumina: Spectroscopic and DFT Study. *ACS Appl. Mat. Interfaces* **2015,** *7*, 26735-26741.
(42) Shi, Q. T.; Huang, Y. Y.; Jing, C. Y., Synthesis, characterization and application of lanthanum-impregnated activated alumina for F removal. *J. Mater. Chem. A* **2013,** *1*, 12797-12803.
(43) Wang, L.; Zhang, J.; Zhao, R.; Li, Y.; Li, C.; Zhang, C., Adsorption of Pb(II) on activated carbon prepared from Polygonum orientale Linn.: Kinetics, isotherms, pH, and ionic strength studies. *Bioresour. Technol.* **2010,** *101*, 5808-5814.
(44) Momčilović, M.; Purenović, M.; Bojić, A.; Zarubica, A.; Ranđelović, M., Removal of lead(II) ions from aqueous solutions by adsorption onto pine cone activated carbon. *Desalination* **2011,** *276*, 53-59.
(45) Sekar, M.; Sakthi, V.; Rengaraj, S., Kinetics and equilibrium adsorption study of lead(II) onto activated carbon prepared from coconut shell. *J. Colloid Interface Sci.* **2004,** *279*, 307-313.
(46) Sreejalekshmi, K. G.; Krishnan, K. A.; Anirudhan, T. S., Adsorption of Pb(II) and Pb(II)-citric acid on sawdust activated carbon: Kinetic and equilibrium isotherm studies. *J. Hazard. Mater.* **2009,** *161*, 1506-1513.
(47) Müller, E. A.; Gubbins, K. E., Molecular simulation study of hydrophilic and hydrophobic behavior of activated carbon surfaces. *Carbon* **1998,** *36*, 1433-1438.
(48) Chen, J. P.; Wu, S.; Chong, K.-H., Surface modification of a granular activated carbon by citric acid for enhancement of copper adsorption. *Carbon* **2003,** *41*, 1979-1986.
(49) Issabayeva, G.; Aroua, M. K.; Sulaiman, N. M. N., Removal of lead from aqueous solutions on palm shell activated carbon. *Bioresour. Technol.* **2006,** *97*, 2350-2355.
(50) Putra, E. K.; Pranowo, R.; Sunarso, J.; Indraswati, N.; Ismadji, S., Performance of activated carbon and bentonite for adsorption of amoxicillin from wastewater: Mechanisms, isotherms and kinetics. *Water Res.* **2009,** *43*, 2419-2430.
(51) Hartman, F. C.; LaMuraglia, G. M.; Tomozawa, Y.; Wolfenden, R., Influence of pH on the interaction of inhibitors with triosephosphate isomerase and determination of the pKa of the active-site carboxyl group. *Biochemistry* **1975,** *14*, 5274-5279.
(52) Li, K.; Wang, X., Adsorptive removal of Pb(II) by activated carbon prepared from Spartina alterniflora: Equilibrium, kinetics and thermodynamics. *Bioresour. Technol.* **2009,** *100*, 2810-2815.
(53) Depci, T.; Kul, A. R.; Önal, Y., Competitive adsorption of lead and zinc from aqueous solution on activated carbon prepared from Van apple pulp: Study in single- and multi-solute systems. *Chem. Eng. J.* **2012,** *200–202*, 224-236.
(54) Zawadzki, J., IR spectroscopy studies of oxygen surface compounds on carbon. *Carbon* **1978,** *16*, 491-

497.
(55) Gasgnier, M., IR spectra of some potassium carboxylates. *J. Mater. Sci. Lett.* **2001,** *20*, 1259-1262.
(56) Lu, Y.; Miller, J. D., Carboxyl Stretching Vibrations of Spontaneously Adsorbed and LB-Transferred Calcium Carboxylates as Determined by FTIR Internal Reflection Spectroscopy. *J. Colloid Interface Sci.* **2002,** *256*, 41-52.
(57) Ibrahim, M.; Nada, A.; Kamal, D. E., Density functional theory and FTIR spectroscopic study of carboxyl group. *Indian Journal of Pure & Applied Physics* **2005,** *43*, 911-917.
(58) Papageorgiou, S. K.; Kouvelos, E. P.; Favvas, E. P.; Sapalidis, A. A.; Romanos, G. E.; Katsaros, F. K., Metal–carboxylate interactions in metal–alginate complexes studied with FTIR spectroscopy. *Carbohydr. Res.* **2010,** *345*, 469-473.
(59) Shin, S.; Jang, J.; Yoon, S. H.; Mochida, I., A study on the effect of heat treatment on functional groups of pitch based activated carbon fiber using FTIR. *Carbon* **1997,** *35*, 1739-1743.
(60) Fanning, P. E.; Vannice, M. A., A DRIFTS study of the formation of surface groups on carbon by oxidation. *Carbon* **1993,** *31*, 721-730.
(61) Gomez-Serrano, V.; Pastor-Villegas, J.; Perez-Florindo, A.; Duran-Valle, C.; Valenzuela-Calahorro, C., FT-IR study of rockrose and of char and activated carbon. *J. Anal. Appl. Pyrolysis* **1996,** *36*, 71-80.
(62) Solum, M. S.; Pugmire, R. J.; Jagtoyen, M.; Derbyshire, F., Evolution of carbon structure in chemically activated wood. *Carbon* **1995,** *33*, 1247-1254.
(63) Terzyk, A. P., The influence of activated carbon surface chemical composition on the adsorption of acetaminophen (paracetamol) in vitro: Part II. TG, FTIR, and XPS analysis of carbons and the temperature dependence of adsorption kinetics at the neutral pH. *Colloids Surf., A* **2001,** *177*, 23-45.
(64) Przepiórski, J., Enhanced adsorption of phenol from water by ammonia-treated activated carbon. *J. Hazard. Mater.* **2006,** *135*, 453-456.
(65) Jia, Y. F.; Thomas, K. M., Adsorption of cadmium ions on oxygen surface sites in activated carbon. *Langmuir* **2000,** *16*, 1114-1122.
(66) Wang, S.-H.; Griffiths, P. R., Resolution enhancement of diffuse reflectance i.r. spectra of coals by Fourier self-deconvolution: 1. C-H stretching and bending modes. *Fuel* **1985,** *64*, 229-236.
(67) Bargar, J. R.; Towle, S. N.; Brown, G. E.; Parks, G. A., XAFS and Bond-Valence Determination of the Structures and Compositions of Surface Functional Groups and Pb(II) and Co(II) Sorption Products on Single-Crystal α-Al2O3. *J. Colloid Interface Sci.* **1997,** *185*, 473-492.
(68) Villalobos, M.; Bargar, J.; Sposito, G., Mechanisms of Pb(II) Sorption on a Biogenic Manganese Oxide. *Environ. Sci. Technol.* **2005,** *39*, 569-576.
(69) Rodriguez-Navarro, C.; Ruiz-Agudo, E.; Burgos-Cara, A.; Elert, K.; Hansen, E. F., Crystallization and Colloidal Stabilization of Ca(OH)2 in the Presence of Nopal Juice (Opuntia ficus indica): Implications in Architectural Heritage Conservation. *Langmuir* **2017,** *33*, 10936-10950.
(70) Burneau, A.; Barres, O.; Gallas, J. P.; Lavalley, J. C., Comparative study of the surface hydroxyl groups of fumed and precipitated silicas. 2. Characterization by infrared spectroscopy of the interactions with water. *Langmuir* **1990,** *6*, 1364-1372.
(71) Pavlov, M.; Siegbahn, P. E. M.; Sandström, M., Hydration of Beryllium, Magnesium, Calcium, and Zinc Ions Using Density Functional Theory. *J. Phys. Chem. A* **1998,** *102*, 219-228.
(72) Jalilehvand, F.; Spångberg, D.; Lindqvist-Reis, P.; Hermansson, K.; Persson, I.; Sandström, M.,

Hydration of the Calcium Ion. An EXAFS, Large-Angle X-ray Scattering, and Molecular Dynamics Simulation Study. *J. Am. Chem. Soc.* **2001,** *123*, 431-441.

(73) Fulton, J. L.; Heald, S. M.; Badyal, Y. S.; Simonson, J. M., Understanding the effects of concentration on the solvation structure of Ca2+ in aqueous solution. I: The perspective on local structure from EXAFS and XANES. *Journal of Physical Chemistry A* **2003,** *107*, 4688-4696.

(74) Dang, L. X.; Schenter, G. K.; Fulton, J. L., EXAFS spectra of the dilute solutions of Ca2+ and Sr2+ in water and methanol. *Journal of Physical Chemistry B* **2003,** *107*, 14119-14123.

(75) Jalilehvand, F.; Spangberg, D.; Lindqvist-Reis, P.; Hermansson, K.; Persson, I.; Sandstrom, M., Hydration of the calcium ion. An EXAFS, large-angle X-ray scattering, and molecular dynamics simulation study. *J. Am. Chem. Soc.* **2001,** *123*, 431-441.

(76) Peak, D.; Ford, R. G.; Sparks, D. L., An in Situ ATR-FTIR Investigation of Sulfate Bonding Mechanisms on Goethite. *J. Colloid Interface Sci.* **1999,** *218*, 289-299.

(77) Ostergren, J. D.; Brown Jr, G. E.; Parks, G. A.; Persson, P., Inorganic Ligand Effects on Pb(II) Sorption to Goethite (α-FeOOH): II. Sulfate. *J. Colloid Interface Sci.* **2000,** *225*, 483-493.

(78) Hug, S. J., In SituFourier Transform Infrared Measurements of Sulfate Adsorption on Hematite in Aqueous Solutions. *J. Colloid Interface Sci.* **1997,** *188*, 415-422.

(79) Topolska, J.; Manecki, M.; Bajda, T.; Borkiewicz, O.; Budzewski, P., Solubility of pyromorphite Pb5(PO4)3Cl at 5–65°C and its experimentally determined thermodynamic parameters. *The Journal of Chemical Thermodynamics* **2016,** *98*, 282-287.

(80) Xie, L.; Giammar, D. E., Chapter 13 Influence of Phosphate on Adsorption and Surface Precipitation of Lead on Iron Oxide Surfaces. In *Developments in Earth and Environmental Sciences*, Mark, O. B.; Douglas, B. K., Eds. Elsevier: 2007; Vol. Volume 7, pp 349-373.

(81) Arai, Y.; Sparks, D. L., ATR-FTIR spectroscopic investigation on phosphate adsorption mechanisms at the ferrihydrite-water interface. *J. Colloid Interface Sci.* **2001,** *241*, 317-326.
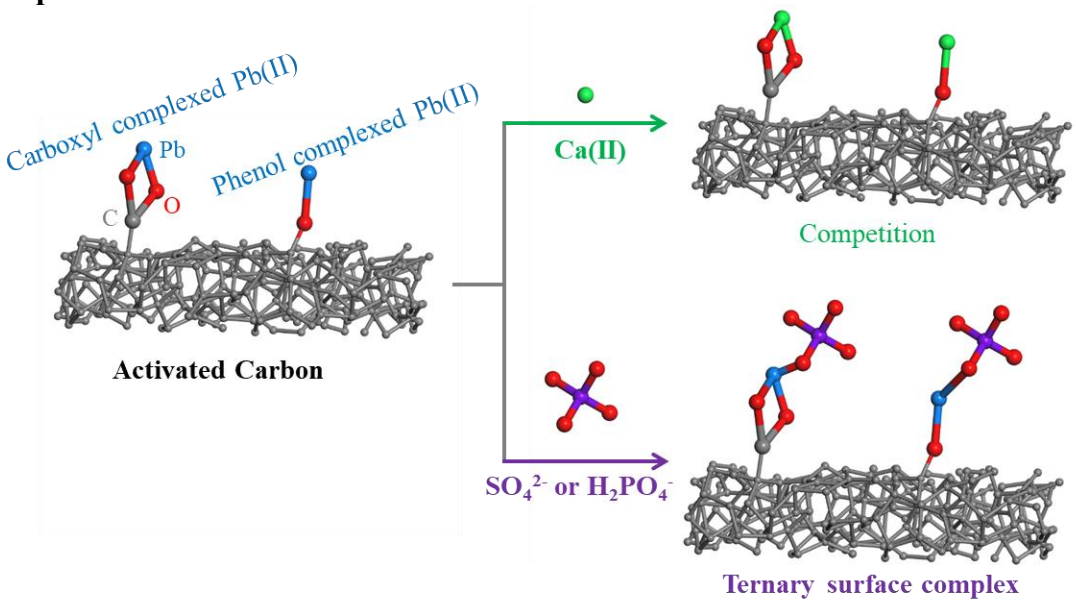
Graphical abstract